Available online at www.sciencedirect.com

ScienceDirect

Mendeleev Commun., 2024, **34**, 572–575

Mendeleev Communications

$NiCo\text{-}Gd_{0.1}Ti_{0.1}Zr_{0.1}Ce_{0.7}O_2$ catalyst for dry reforming and partial oxidation of methane: effect of NiCo applying method on the conversion of methane to synthesis gas

Igor V. Zagaynov,*[a] Alexey S. Loktev,[b] Anatoly A. Konovalov,[a] Anton A. Klimashin,[a] Olga S. Antonova[a] and Alexey G. Dedov[b,c]

[a] *A. A. Baikov Institute of Metallurgy and Materials Science, Russian Academy of Sciences, 119334 Moscow, Russian Federation. E-mail: igorscience@gmail.com*

[b] *A. V. Topchiev Institute of Petrochemical Synthesis, Russian Academy of Sciences, 119334 Moscow, Russian Federation*

[c] *National University of Oil and Gas 'Gubkin University', 117917 Moscow, Russian Federation*

DOI: 10.1016/j.mencom.2024.06.034

A series of catalysts based on mesoporous ceria solid solutions containing NiCo active component was synthesized *via* co-precipitation, impregnation, hydrothermal and core–shell (sol–gel) methods and applied to partial oxidation and dry reforming of methane. In the co-precipitated and impregnated catalysts, a better NiCo dispersion and a stronger interaction between NiCo species and the ceria-based support in comparison with other catalysts were observed, which affected activity and selectivity. Thus, simpler methods of applying the active component were more advantageous owing to the manifestation of strong metal–support interactions.

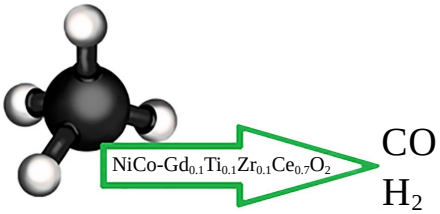

Keywords: ceria, dry reforming of methane, effect of preparation, NiCo, partial oxidation of methane, syngas.

Methane conversion is one of the modern large-scale industrial processes for the oxidative conversion of natural gas to form the synthesis gas. This gas mixture is used as a source of hydrogen for the manufacture of petrochemical products and intermediates.[1,2] Various processes of methane converting into synthesis gas catalyzed by heterogeneous nickel-containing systems with using oxidants (H_2O, O_2 and CO_2) at high temperatures (750–950 °C) are characterized by high energy consumption and deactivation of the catalyst, mainly due to carbon deposition on the surface of the catalyst and sintering of active components.[3,4] Different methods to overcome this problem have been proposed: using promoters for metal active phases and support, utilization of a sulfur passivated reforming process to eliminate carbon deposition by poisoned catalysts, changing catalysts preparation methods and conditions to improve physicochemical properties of the catalysts.[5,6] Ni-based catalysts have been widely investigated owing to their low costs and relatively high activity. In many studies, the effects of active phase promoters were evaluated on Ni properties and it was revealed that a NiCo bimetallic catalyst with a certain Ni/Co ratio was the best option.[7–12] A homogeneous alloy of Co and Ni and low Ni substitution of Co dramatically improved catalyst activity and stability. The investigation of the metal additives to Ni has shown higher catalytic activity of NiCo compared with monometallic and other bimetallic combinations. It is clear that bi- and trimetallic catalysts may exhibit superior performance in reforming of methane in comparison with the corresponding monometallic catalysts.[13–15]

The catalyst synthesis methods strongly affect the physicochemical properties and performance of the catalyst. However, the data on the effect of the method of applying the active component differs; the catalysts obtained by co-precipitation method can be either more active than those obtained by impregnation, plasma treatment, atomic layer deposition, sol–gel, microemulsion and other methods or *vice versa*.[16–22] But in all the works it was noted that the higher catalytic activities were due to the partial incorporation of nickel into the support, which resulted in the higher dispersion and stronger metal–support interaction. It indicates that a proper choice of preparation method imparts certain textural properties, support activity and enhanced metal–support interaction ensuring higher catalytic activity and lower carbon deposition.

Therefore, the present work is focused on developing stable POM (partial oxidation of methane) and DRM (dry reforming of methane) catalysts based on mesoporous ceria solid solutions containing NiCo active component applied by various methods: co-precipitation, impregnation, hydrothermal and core–shell approaches. The choice of such complex support ($Gd_{0.1}Ti_{0.1}Zr_{0.1}Ce_{0.7}O_2$) is related to the necessity to stabilize the ceria structure for operations at temperatures above 700 °C and on the basis of previous studies.[9,13,14,22] The effects of various dopants and their ratios on the catalytic properties were studied, therefore the best system was selected.

The main characteristics of the synthesized samples are presented in Table 1. Activity was assessed in the POM and DRM reactions (Table 2). Whereas the DRM reaction is mostly

Table 1 Main characteristics of fresh and used catalysts NiCo-$Gd_{0.1}Ti_{0.1}Zr_{0.1}Ce_{0.7}O_2$ (Ni/Co = 80/20 mol/mol) synthesized by various methods (f – fresh, p – used in partial oxidation of methane and d – used in dry reforming of methane).

Sample no.	Method	Active site phase (wt%)	d_{XRD}/nm (support)	d_{XRD}/nm (active site)	S_{BET}/ $m^2\ g^{-1}$
1f	co-precipitation	4.7 (NiCo)O	9	10 (NiCo)O	72
1p		8.3 (NiCo)O	19	16 (NiCo)O	6
1d		3.7 NiCo,	22	22 NiCo,	6
		3.0 (NiCo)O		20 (NiCo)O	
2f	impregnation	8 (NiCo)O	10	8 (NiCo)O	68
2p		7.9 (NiCo)O	16	16 (NiCo)O	13
2d		2.3 NiCo,	20	22 NiCo,	14
		5.5 (NiCo)O		21 (NiCo)O	
3f	hydrothermal	12.1 (NiCo)O	10	18 (NiCo)O	72
3p		0.7 NiCo,	17	30 NiCo,	13
		10.3 (NiCo)O		24 (NiCo)O	
3d		6.7 NiCo	15	41 NiCo	14
4f	core–shell	11.7 (NiCo)O	10	36 (NiCo)O	70
4p		0.9 NiCo,	16	30 NiCo,	15
		8.5 (NiCo)O		21 (NiCo)O	
4d		8.9 NiCo	17	37 NiCo	16

Table 2 Catalytic activity of samples in POM or DRM processes at 900 °C.

Sample no.	CH_4 conversion (%)	O_2 (POM) or CO_2 (DRM) conversion (%)	CO yield (%)	H_2 yield (%)	H_2/CO
1f	98 (POM)	98 (POM)	97 (POM)	95 (POM)	2.0 (POM)
	93 (DRM)	93 (DRM)	93 (DRM)	78 (DRM)	0.9 (DRM)
2f	96 (POM)	99 (POM)	93 (POM)	93 (POM)	2.0 (POM)
	98 (DRM)	99 (DRM)	98 (DRM)	98 (DRM)	1.0 (DRM)
3f	95 (POM)	99 (POM)	89 (POM)	89 (POM)	2.0 (POM)
	96 (DRM)	98 (DRM)	95 (DRM)	95 (DRM)	1.0 (DRM)
4f	98 (POM)	99 (POM)	93 (POM)	93 (POM)	2.0 (POM)
	97 (DRM)	99 (DRM)	97 (DRM)	97 (DRM)	1.0 (DRM)

endothermic, the methane conversion raises by increasing the reaction temperature. At 900 °C, the conversions and product yields are close. However, in exothermic POM reaction, the sample obtained by the co-precipitation method turned out to be somewhat more active and selective (Table S1), while in DRM reaction, it was a catalyst obtained by the impregnation method. Thus, simpler methods for applying the active component were more advantageous. The ratio of hydrogen to carbon monoxide is an important indicator. It is close to the theoretical value for all systems and processes. One of the reasons for the deviation may be the occurrence of reverse water gas reaction.[23] The stability of catalysts has been also evaluated (see Online Supplementary Materials, Figure S1) and the results demonstrate that highly efficient and stable catalysts have been formed. The developed catalyst was more active and stable than industrial catalysts, *e.g.*, Katalco 57-4 (16% Ni/Al_2O_3). Compared with the catalysts reported in the previous works, the catalytic activity of our materials is characterized by a slightly higher conversion of CH_4 and CO_2 in DRM[24,25] and selectivity of H_2/CO in POM,[26] even without the addition of noble metals.[27]

The structural changes of the as-prepared and spent catalysts were investigated using XRD (see Figure 1 and Table 1). All fresh catalysts exhibited a fluorite ceria structure of support and bimetallic oxide (NiCo)O (type *B*1, *cF*8) of the active component. Moreover, the amount of active phase in the co-precipitation method was significantly lower than when applying the active component by any other method. Apparently, some of the nickel and cobalt enter the ceria lattice, forming a solid solution.

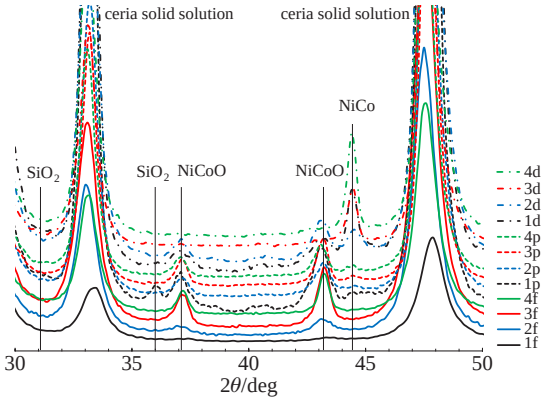

Figure 1 XRD patterns of fresh catalysts and used after POM and DRM. SiO_2 from quartz pieces packing.

Shifting in the XRD peaks in the substituted support in comparison with the others and the values of lattice parameter have been found to reduce upon the substitution.[9,14,23,28] That is also typical for the impregnation method, part of the metal oxides are present on the surface in amorphous phase or the form of the highly dispersed nanoparticles.[29] The smaller crystallite size of the active site (d_{XRD}) also confirms the patterns listed above. After catalysis, there is a slight increase in the crystallite sizes of both the support and the active phase due to sintering. As a rule, after POM the oxide phase of the active component remains, and after DRM the metallic phase does. Moreover, after POM, in hydrothermal and core–shell samples, a metal phase also appears, apparently owing to the larger particle size of the active sites (the crystallite size of the support is comparable for all systems). It is also worth noting that the residual NiCoO content in catalyst 2d is associated with the manifestation of a strong metal–support interaction.[30,31] It is demonstrated that Ni and/or Co ions in complex oxide catalysts can be reduced during POM or DRM processes to provide metallic nanoparticles and this agrees with TPR (temperature programmed reduction) analysis data.[16,32] The reduction of the active species became difficult, indicating enhanced interaction between support and NiCo species. Earlier works report that Ni(Co) ions can be incorporated into the ceria-based lattice to form a Ni(Co)–Ce–O solid solution, thus generating oxygen vacancies and reducible oxygen species. These rich interfacial sites make it easier to remove adsorbed oxygen by CH_x and it shows a similar trend for the catalysts activity.[33,34]

The evolution of the surface texture of catalysts before and after catalytic testing has been also observed. In addition to a decrease in specific surface area (Table 1), there is also a change in the shape of adsorption–desorption curves (Figure S2) and pore size distributions (Figure S3). The synthesized samples are mesoporous, which is proved by type IV adsorption isotherm with an H2–H3 hysteresis loop. Changes in pore size distribution and the shape of hysteresis loop occurred during the catalytic process: from monomodal (2–10 nm, H2–H3 type) to polymodal (2–70 nm, H3 type – characteristic of aggregate particles with no uniform size and shape). Relatively small pores disappear first upon heat treatment, whereas the position and height of the other pore size distribution peaks have changed far more. Sample 1, obtained by co-precipitation, has undergone the most significant changes. High-temperature treatment of catalyst in the reaction conditions results in the significant decrease in their surface area due to the phase transformation (in DRM) and intensification of sintering processes. At higher temperatures reaction conditions, catalysts partially retain their mesoporosity, and the loss of surface area is due to agglomeration and the collapse of the pore structure, which is not related to catalytic processes, it is only the temperature factor that affects it.[35–37]

The thermogravimetric experiment was conducted to determine the quantity of carbon deposited on spent catalysts in air (see Figure S4). A slight weight loss occurs in the low-temperature region (100–350 °C) due to the desorption of water and some volatile intermediate products, as well as the oxidation of amorphous and filamentous carbon. In the region of 350–700 °C two processes occur simultaneously. Weight loss is due to the combustion of graphitic and nanotube carbon. The weight of the spent catalysts increases in parallel, which is associated with the oxidation of the metallic NiCo active component.[38,39] It is also possible that the resulting metal phase of the active component oxidizes, resulting in a slight weight gain. No more changes occurred after 700 °C. If coke deposition is only evaluated by the exo-effect at 200–300 °C, then the catalyst made by the core–shell method is most susceptible to this effect. The thermograms of sample 1 after the processes of POM and DRM are shown in Figure S5: in comparison to the described effects in catalysts after DRM, there is only a slight deposition of amorphous carbon in POM, which is naturally due to the presence of oxygen in the mixture. Ceria-based supports have a strong impact on the resistance of the catalyst to coking. In contrast to other supports, the high oxygen mobility and storage capacity, basic and redox properties of ceria systems help to eliminate carbon deposits.[40]

As can be seen in the SEM photographs (see Online Supplementary Materials, Figure S6, catalyst 2), no significant changes in particle aggregates occur after catalysis. Thus, no carbon was detected in different areas of the sample 2p; in turn, after DRM (2d), a small deposit of carbon similar to a graphite structure was found. The surface composition was studied by the EDS method. The Gd/Ti/Zr/Ce ratio remained close to 1/1/1/7 in all samples, and the Co/Ni ratio in fresh samples was 1/2 (probably a part of the core–shell structure and therefore the active phase have been enriched with cobalt). After POM and DRM reactions it became 1/4 and 1/3.6, respectively, (as a result of the reaction, the formation of a metallic phase and 'the conditional distribution of elements' occurs).

Thus, the deactivation of catalysts in methane conversion can be attributed to two factors: coke depositing on the active sites as well as their sintering. Bimetallic catalysts improve $O_2(CO_2)$ activation to form CO and adsorbed oxygen. CO is produced by combining the adsorbed oxygen and CH_x. $O_2(CO_2)$ activation can be improved by the support, particularly a ceria-containing one, inasmuch as its oxygen vacancies generate C–O or formate (in DRM) intermediates.[9,14,28] The CH_xO has also been regarded as a critical intermediate. The reaction pathway from CH_x to CH_xO is favorable on the active site with NiCo–O coordination owing to the superior mobility of ceria surface lattice oxygen atoms.[41,42] The advantage of the proposed catalysts, ceteris paribus, is the simplicity of their preparation, *i.e.*, co-precipitation or impregnation methods without any additives. Results demonstrate that ceria-based support and a NiCo bimetallic active site prevent intensive coke formation.

An effective and promising strategy for the rational design of catalysts to achieve highly stable product for partial oxidation of methane and dry reforming of methane was developed. In the POM reaction, a catalyst obtained *via* the co-precipitation method was more active and selective, while in the DRM reaction, it was a catalyst obtained *via* the impregnation method. Thus, simpler methods of applying the active component were more advantageous. It indicated the crucial role of the intimate interaction between NiCo active sites and oxygen vacancies in determining the specific activity of ceria-based support. Despite carbon deposition, there was no decrease in conversion or syngas production.

This work was partially supported by the Ministry of Science and Higher Education of the Russian Federation within the governmental orders and the state funding of IMET RAS and TIPS RAS.

Online Supplementary Materials

Supplementary data associated with this article can be found in the online version at doi: 10.1016/j.mencom.2024.06.034.

References

1 J. Rostrup-Nielsen and L. J. Christiansen, *Concepts in Syngas Manufacture*, Imperial College Press, London, 2011.
2 N. V. Kolesnichenko, N. N. Ezhova and Yu. M. Snatenkova, *Russ. Chem. Rev.*, 2023, **92**, RCR5079.
3 B. C. Enger, R. Lødeng and A. Holmen, *Appl. Catal., A*, 2008, **346**, 1.
4 L. P. Teh, H. D. Setiabudi, S. N. Timmiati, M. A. A. Aziz, N. H. R. Annuar and N. N. Ruslan, *Chem. Eng. Sci.*, 2021, **242**, 116606.
5 M. Usman, W. M. A. Wan Daud and H. F. Abbas, *Renewable Sustainable Energy Rev.*, 2015, **45**, 710.
6 I. V. Zagaynov, *Energy Fuels*, 2021, **35**, 9124.
7 J. Xu, W. Zhou, Z. Li, J. Wang and J. Ma, *Int. J. Hydrogen Energy*, 2009, **34**, 6646.
8 J. Xin, H. Cui, Z. Cheng and Z. Zhou, *Appl. Catal., A*, 2018, **554**, 95.
9 I. V. Zagaynov, A. S. Loktev, I. E. Mukhin, A. G. Dedov and I. I. Moiseev, *Mendeleev Commun.*, 2017, **27**, 509.
10 L. Chen, Q. Zhu and R. Wu, *Int. J. Hydrogen Energy*, 2011, **36**, 2128.
11 T. H. Lim, S. J. Cho, H. S. Yang, M. H. Engelhard and D. H. Kim, *Appl. Catal., A*, 2015, **505**, 62.
12 B. AlSabban, L. Falivene, S. M. Kozlov, A. Aguilar-Tapia, S. Ould-Chikh, J.-L. Hazemann, L. Cavallo, J.-M. Basset and K. Takanabe, *Appl. Catal., B*, 2017, **213**, 177.
13 I. V. Zagaynov, A. S. Loktev, A. L. Arashanova, V. K. Ivanov, A. G. Dedov and I. I. Moiseev, *Chem. Eng. J.*, 2016, **290**, 193.
14 I. V. Zagaynov, A. S. Loktev, I. E. Mukhin, A. A. Konovalov, A. G. Dedov and I. I. Moiseev, *Mendeleev Commun.*, 2019, **29**, 22.
15 V. Ponec and G. C. Bond, *Catalysis by Metals and Alloys*, Elsevier, Amsterdam, 1995.
16 J. Chen, Q. Wu, J. Zhang and J. Zhang, *Fuel*, 2008, **87**, 2901.
17 D.-W. Jeong, W.-J. Jang, J.-O. Shim, H.-S. Roh, I. H. Son and S. J. Lee, *Int. J. Hydrogen Energy*, 2013, **38**, 13649.
18 T. Odedairo, J. Chen and Z. Zhu, *Catal. Commun.*, 2013, **31**, 25.
19 H. O. Seo, J. K. Sim, K.-D. Kim, Y. D. Kim, D. C. Lim and S. H. Kim, *Appl. Catal., A*, 2013, **451**, 43.
20 M. Boutonnet, S. Lögdberg and E. E. Svensson, *Curr. Opin. Colloid Interface Sci.*, 2008, **13**, 270.
21 H.-W. Kim, K.-M. Kang, H.-Y. Kwak and J. H. Kim, *Chem. Eng. J.*, 2011, **168**, 775.
22 I. V. Zagaynov, A. S. Loktev, I. E. Mukhin, A. A. Konovalov and A. G. Dedov, *Mendeleev Commun.*, 2022, **32**, 129.
23 P. K. Yadav and S. Sharma, *Fuel*, 2024, **358**, 130163.
24 I. Luisetto, S. Tuti, C. Battocchio, S. Lo Mastro and A. Sodo, *Appl. Catal., A*, 2015, **500**, 12.
25 H. Ay and D. Üner, *Appl. Catal., B*, 2015, **179**, 128.
26 T. P. Maniecki, K. Bawolak, D. Gebauer, P. Mierczynski and W. K. Jozwiak, *Kinet. Catal.*, 2009, **50**, 138.
27 N. H. Elsayed, N. R. M. Roberts, B. Joseph and J. N. Kuhn, *Appl. Catal., B*, 2015, **179**, 213.
28 E. Yang, E. Nam, Y. Jo and K. An, *Appl. Catal., B*, 2023, **339**, 123152.
29 Y. Zhao, L. Qi, Z. Cheng and Z. Zhou, *Ind. Eng. Chem. Res.*, 2022, **61**, 12978.
30 Y. Wang, L. Xiao, Y. Qi, J. Yang, Y.-A. Zhu and D. Chen, *J. Phys. Chem. C*, 2020, **124**, 2501.
31 Z. Lian, S. O. Olanrele, C. Si, M. Yang and B. Li, *J. Phys. Chem. C*, 2020, **124**, 5118.
32 T. Sukonket, A. Khan, B. Saha, H. Ibrahim, S. Tantayanon, P. Kumar and R. Idem, *Energy Fuels*, 2011, **25**, 864.
33 P. Hongmanorom, J. Ashok, P. Chirawatkul and S. Kawi, *Appl. Catal., B*, 2021, **297**, 120454.
34 N. Rui, X. Zhang, F. Zhang, Z. Liu, X. Cao, Z. Xie, R. Zou, S. D. Senanayake, Y. Yang, J. A. Rodriguez and C.-J. Liu, *Appl. Catal., B*, 2021, **282**, 119581.
35 L. Xu, H. Song and L. Chou, *Int. J. Hydrogen Energy*, 2012, **37**, 18001.
36 I. V. Zagaynov, *Ceram. Int.*, 2015, **41**, 8730.

37 E. V. Matus, O. B. Sukhova, M. A. Kerzhentsev, I. Z. Ismagilov, S. A. Yashnik, V. A. Ushakov, T. V. Larina, E. Yu. Gerasimov, O. A. Stonkus, A. P. Nikitin, L. Li and Z. R. Ismagilov, *Catal. Lett.*, 2024, **154**, 2197.
38 A. S. Al-Fatesh, Y. Arafat, S. O. Kasim, A. A. Ibrahim, A. E. Abasaeed and A. H. Fakeeha, *Appl. Catal., B*, 2021, **280**, 119445.
39 C. M. Damaskinos, J. Zavašnik, P. Djinović and A. M. Efstathiou, *Appl. Catal., B*, 2021, **296**, 120321.
40 T. Montini, M. Melchionna, M. Monai and P. Fornasiero, *Chem. Rev.*, 2016, **116**, 5987.
41 Z. Rao, K. Wang, Y. Cao, Y. Feng, Z. Huang, Y. Chen, S. Wei, L. Liu, Z. Gong, Y. Cui, L. Li, X. Tu, D. Ma and Y. Zhou, *J. Am. Chem. Soc.*, 2023, **145**, 24625.
42 Y. Tang, Y. Wei, Z. Wang, S. Zhang, Y. Li, L. Nguyen, Y. Li, Y. Zhou, W. Shen, F. F. Tao and P. Hu, *J. Am. Chem. Soc.*, 2019, **141**, 7283.

Received: 6th February 2024; Com. 24/7388